Actin Polymerization and Depolymerization Coupled to Cooperative Hydrolysis

Xin Li,[1,2] Jan Kierfeld,[3] and Reinhard Lipowsky[1]

[1]*Theory & Bio-Systems, Max Planck Institute of Colloids and Interfaces, 14424 Potsdam, Germany**

[2]*Key Laboratory of Frontiers in Theoretical Physics, ITP, CAS, Beijing 100190, China*

[3]*Physics Department, TU Dortmund University, 44221 Dortmund, Germany*

(Received 18 February 2009; published 23 July 2009)

The hydrolysis of adenosine triphosphate (ATP) during actin (de)polymerization consists of two subprocesses, ATP cleavage and phosphate (P_i) release, which involve three nucleotide states of each actin protomer. A new theoretical model that explicitly incorporates these different subprocesses and states is introduced and compared with recent experimental data for actin depolymerization. These data can be explained by strongly cooperative ATP cleavage followed by strongly cooperative P_i release but are incompatible with random and/or vectorial subprocesses as proposed previously.

DOI: 10.1103/PhysRevLett.103.048102 PACS numbers: 87.16.Ka, 87.16.A−

The (de)polymerization of actin is essential for many biological processes such as cell adhesion, locomotion, and division, all of which are coupled to ATP hydrolysis [1]. To elucidate the underlying molecular processes, a large number of in vitro experiments has been performed: actin *structure* has been studied by diffraction methods [2–4] and electron microscopy [5,6], actin *dynamics* by spectroscopy of filament solutions [7–12] and fluorescence microscopy of individual filaments [13,14].

Actin monomers (or G-actin) assemble into filaments with two distinct ends, a barbed, fast growing end and a pointed, slow growing end. Each monomer contains one nucleotide binding cleft where ATP is transformed into adenosine diphosphate (ADP) and inorganic phosphate (P_i) via two subprocesses: ATP cleavage, which produces ADP/P_i-actin, and P_i release, which leads to ADP-actin. ATP cleavage is extremely slow for actin monomers but is strongly increased after the monomer has been incorporated into a filament and turned into a protomer (or filament subunit). Thus, the nucleotide binding cleft must be affected by the transformation from the monomer to the protomer. However, the underlying molecular mechanisms are not understood and have been controversial for many years.

Actin filaments (or F-actin) cannot be crystallized, and the conventional model for their structure has been obtained by mapping high-resolution x-ray structures of G-actin crystals into lower-resolution structures of oriented F-actin gels [15]. High-resolution x-ray structures of G-actin crystals with bound ATP [3,4] and bound ADP [2,4] indicated structural differences between ATP-actin and ADP-actin. F-actin exhibits some structural plasticity as observed by electron microscopy, which showed that actin polymerization leads initially to many protomers that are tilted away from the conventional helix structure [5,6]. Very recently, fluorescence microscopy of individual filaments provided rather direct evidence for the structural plasticity of depolymerizing filaments [14]. In these latter experiments, the time evolution of the filaments was observed to exhibit several dynamic phases with distinct depolymerization rates; see Fig. 1. These observations were interpreted in terms of structural rearrangements of the filaments from an initially disordered state to the conventional helix structure.

In this Letter, we study the consistency of these new experimental data [14] with our knowledge about the coupling between actin (de)polymerization and ATP hydrolysis. The latter coupling involves three well-established properties: (i) Each protomer in the filament can attain three different nucleotide states, namely, ATP-actin, ADP/P_i-actin, and ADP-actin. This property is a direct consequence of the experimental observation that P_i release is relatively slow [11]; (ii) Detachment of ADP/P_i-actin and ADP-actin from the pointed end is much slower than from the barbed end [13]. Indeed, the detachment rate at the pointed end as measured in [14] was only about 0.1 protomers/s, which implies that the different phases in Fig. 1 must reflect different detachment processes at the barbed end; and (iii) The detachment rate of ADP/P_i-actin from the barbed end is much smaller

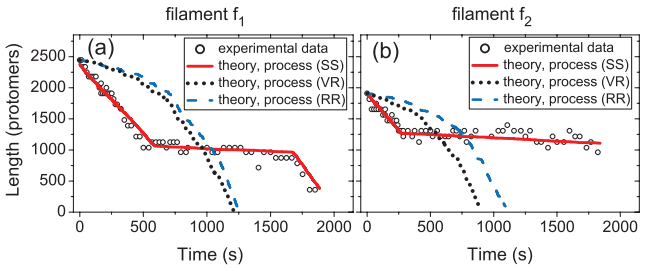

FIG. 1 (color). Depolymerization of two actin filaments, denoted by f_1 and f_2, as recently observed in Ref. [14]: Length of (a) f_1 and (b) f_2 as a function of time. The experimental data [14] are well described by the hydrolysis process (SS) introduced here, which consists of strongly cooperative ATP cleavage followed by strongly cooperative P_i release but are incompatible with the two processes (RR) and (VR) that have been previously proposed in the literature as explained in the text.

than the detachment rate of both ATP-actin and ADP-actin from the same end [13].

When we combine these three noncontroversial properties of actin (de)polymerization with possible mechanisms for ATP cleavage and P_i release, we find that the depolymerization phases as displayed in Fig. 1 can be explained by *strongly* cooperative ATP cleavage followed by *strongly* cooperative P_i release, a combination that we abbreviate as (SS). During polymerization, the process (SS) produces actin filaments that consist of three different segments: an ATP-actin cap close to the barbed end, an intermediate segment that consists primarily of ADP/P_i-actin, and a filament core of ADP-actin. The successive depolymerization of these three filament segments leads to the three dynamic phases shown in Fig. 1. In this way, we provide a relatively simple explanation for the surprising behavior observed in [14].

The process (SS) must be distinguished from two other processes that have been previously discussed in the literature: Several groups emphasized the process (RR) corresponding to "*random* ATP cleavage followed by *random* P_i release" [12,13,16,17] whereas other groups considered the process (VR) corresponding to "*vectorial* cleavage [9,18] followed by *random* P_i release" [11]. Inspection of Fig. 1 shows that both processes (RR) and (VR) are incompatible with the data in [14].

For random ATP cleavage, all ATP-actin protomers exhibit the same cleavage rate irrespective of their local neighborhoods within the filament as illustrated in Fig. 2(a). Vectorial (or sequential) cleavage, on the other hand, is restricted to the domain boundary between the ATP-actin cap at the barbed end and the core of the filament; see Fig. 2(b). Vectorial and random cleavage may be considered as limiting cases of the cooperative cleavage process shown in Fig. 2(c). Random, vectorial, and cooperative P_i release from the ADP/P_i-actin protomers will be defined in an analogous way; see further below.

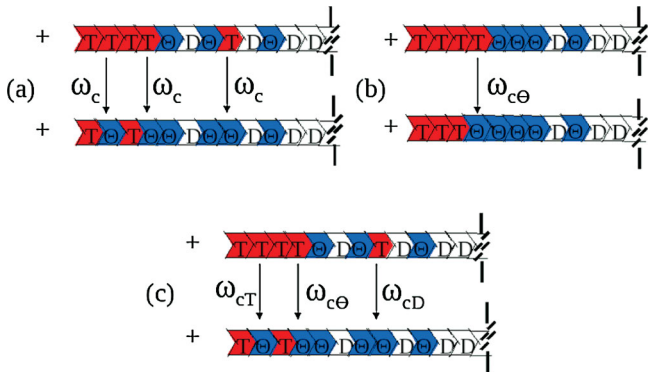

FIG. 2 (color). (a) Random cleavage of ATP-actin protomers (T, red) to ADP/P_i-actin (Θ, blue) in the presence of ADP-actin protomers (D, white) with all cleavage rates being equal to ω_c irrespective of the local neighborhood; (b) Vectorial cleavage with rate $\omega_{c\Theta}$ restricted to the TΘ or TD domain boundary of the T cap; and (c) Cooperative cleavage with three cleavage rates ω_{cT}, $\omega_{c\Theta}$, and ω_{cD} depending on the local neighborhood of the T protomer to be cleaved. Random, vectorial, and cooperative P_i release are defined in an analogous way.

In the context of actin polymerization, cooperative hydrolysis of ATP has been discussed in [9,10]. Furthermore, cooperative hydrolysis of GTP has been used to explain the abrupt transitions of microtubules from growing to shrinking states [19]. In all of these previous models for cooperative hydrolysis, the protomers could attain only two nucleotide states. In contrast, our theory takes all three nucleotide states of actin into account and distinguishes ATP cleavage from P_i release.

Our article is organized as follows. First, we introduce our theoretical model for actin (de)polymerization and discuss the possible domain patterns of actin protomers. Second, we study several steady state quantities and show that the different processes (RR), (VR), and (SS) are rather difficult to distinguish via these quantities. Finally, we apply our model to depolymerization after dilution and derive the corresponding time evolution of the filament length as shown in Fig. 1.

Description of protomer patterns.—We will now abbreviate the three protomer species ATP-actin, ADP/P_i-actin, and ADP-actin by T, Θ, and D, respectively. At any time t, the state of the filament is defined by the spatial pattern of T, Θ, and D protomers; see Fig. 2. This pattern evolves in time according to a continuous-time Markov process with transition rates ω_{ij} from state i to state j. This implies (i) that the dwell (or waiting) time τ_i of the system in state i is governed by the probability

$$\text{Prob}\,(\tau_i > t) = \exp[-t/\langle\tau_i\rangle] \;\text{ with }\; \langle\tau_i\rangle \equiv 1\Big/\sum_j \omega_{ij} \quad (1)$$

and (ii) that the transition occurs to state j with probability $\pi_{ij} = \langle\tau_i\rangle\omega_{ij}$ [20].

The transition rate for filament elongation is equal to the attachment rate of a single T monomer to the barbed end and given by $\kappa_{on}C_T$ with rate constant κ_{on} and molar concentration C_T of ATP actin. The detachment rates for a T, Θ, and D protomer from the barbed end are denoted by $\omega_{off,T}$, $\omega_{off,\Theta}$, and $\omega_{off,D}$, respectively. Once a T monomer has been attached to the filament and turned into a T protomer, its ATP molecule is cleaved into ADP/P_i and the P_i is subsequently released.

Cooperative ATP cleavage and P_i *release.*— Each protomer has a polar structure with a "pointed" and a "barbed" side as indicated in Fig. 2. The binding cleft for ATP is located at the pointed side of the protomer which points towards the core of the filament. Therefore, the ATP cleavage rate of a certain T protomer may depend, in general, on the next protomer that separates the T protomer from the filament core. Thus, we distinguish the three local neighborhoods TT, TΘ, and TD with the corresponding ATP cleavage rates ω_{cT}, $\omega_{c\Theta}$, and ω_{cD} [21]. We take $\omega_{c\Theta} = \omega_{cD}$; see [22], and use the parametrization

$$\omega_{c\Theta} = \omega_{cD} \equiv \omega_c \quad \text{and} \quad \omega_{cT} \equiv \rho_c\omega_c, \quad (2)$$

which defines the dimensionless cleavage parameter ρ_c that can attain the values $0 \leq \rho_c \leq 1$. For $\rho_c = 1$, all three rates are equal to ω_c corresponding to random cleavage. For $\rho_c = 0$, the ATP cleavage rate ω_{cT} adjacent to a neighboring T protomer vanishes, and cooperative cleavage reduces to vectorial cleavage.

For cooperative P_i release from a Θ protomer, we distinguish the three local neighborhoods ΘT, $\Theta\Theta$, and ΘD and the corresponding P_i release rates ω_{rT}, $\omega_{r\Theta}$, and ω_{rD}. We take $\omega_{rT} = \omega_{r\Theta}$ and use the parametrization

$$\omega_{rD} \equiv \omega_r \quad \text{and} \quad \omega_{rT} = \omega_{r\Theta} \equiv \rho_r \omega_r \tag{3}$$

with the dimensionless release parameter ρ_r that can attain the values $0 \leq \rho_r \leq 1$. For $\rho_r = 1$, all three rates are equal to ω_r corresponding to random P_i release. For $\rho_r = 0$, the P_i release rates ω_{rT} and $\omega_{r\Theta}$ adjacent to a neighboring T and Θ monomer vanish, and cooperative P_i release reduces to vectorial P_i release.

Threshold concentrations for vectorial subprocesses.—Vectorial cleavage with $\rho_c = 0$ is characterized by a T cap at the barbed end. As shown in [22], this cap has a finite length for small actin concentrations C_T but grows continuously when C_T exceeds the threshold value

$$C_{T,c} \equiv (\omega_c + \omega_{off,T})/\kappa_{on}. \tag{4}$$

Vectorial P_i release with $\rho_r = 0$ leads to protomer patterns with one or no ΘD domain boundary. The average separation of this domain boundary from the barbed end grows continuously if C_T exceeds another threshold concentration, $C_{T,r}$, which satisfies the implicit equation

$$\omega_r = \kappa_{on} C_{T,r} - P_T(1)\omega_{off,T} - [1 - P_T(1)]\omega_{off,\Theta}, \tag{5}$$

where $P_T(1)$ is the probability that the first protomer at the barbed end is a T protomer; see Fig. (5) in [22].

Different hydrolysis processes. We will now describe and compare the behavior of growing and shrinking actin filaments for the three processes denoted by (RR), (VR), and (SS) with transition rates as given in Table I. The first process (RR) represents random ATP cleavage with cleavage parameter $\rho_c = 1$ followed by random P_i release with release parameter $\rho_r = 1$. The corresponding transition rates in Table I have been deduced in [7,12,13] for a physiological buffer containing 1 or 2 mM $MgCl_2$ and 50 or 100 mM KCl. The second process (VR) is based on vectorial ATP cleavage with $\rho_c = 0$ followed by random P_i release with $\rho_r = 1$. The (VR) transition rates in Table I have been deduced in [9,11] for a buffer containing 1 mM $MgCl_2$ and no KCl. The third process (SS) represents strongly cooperative cleavage with $\rho_c = 3/10^6$ followed by strongly cooperative P_i release with $\rho_r = 2/10^6$ [23]. The latter parameters have been obtained here from a detailed comparison with the experiments in [14], see below. The buffer used in these latter experiments contained 2 mM $MgCl_2$ as well as 50 mM KCl, similar to but not identical with the one in [7,12].

TABLE I. Transition rates for process (RR) [12,13], for process (VR) [9,11], and for process (SS) introduced here. The rate constant κ_{on} is in units of $1/\mu M$ s, all rates ω are in units of $1/s$, and the parameters ρ_c and ρ_r are dimensionless.

	κ_{on}	$\omega_{off,T}$	$\omega_{off,\Theta}$	$\omega_{off,D}$	ω_c	ρ_c	ω_r	ρ_r
(RR)	11.6	1.4	0.2	5.4	0.3	1	0.003	1
(VR)	1.7	5.1	0.2	5.0	13.6	0	0.003	1
(SS)	11.6	2.2	0.1	2.7	1.0	$3/10^6$	0.57	$2/10^6$

Steady state properties.—We first determined several steady state fluxes as functions of actin concentration C_T: the filament growth rate; see Fig. (6) in [22], the total ATP cleavage flux J_c, and the total P_i release flux J_r. In Fig. 3, the concentration dependencies of the two fluxes J_c and J_r are compared for the three processes (RR), (VR), and (SS). For the vectorial process (VR), the flux J_c attains the constant value $J_c = \omega_c = 13.6/s$ for $C_T > C_{T,c} = 11.0\mu M$ as experimentally observed in [9].

For each position x along the filament, one can define the protomer densities $P_T(x)$, $P_\Theta(x)$, and $P_D(x)$, which represent the probabilities that this protomer belongs to the species T, Θ, and D, respectively. The densities $P_T(x)$ and $P_D(x)$ decrease and increase monotonically with x, whereas $P_\Theta(x)$ exhibits a maximum at intermediate values of x; see Fig. (7) in [22].

The average numbers $\langle N_T \rangle$ and $\langle N_\Theta \rangle$ of T and Θ protomers are obtained by integrating the density profiles $P_T(x)$ and $P_\Theta(x)$ over x. The concentration dependence of these average numbers is displayed in Fig. 4. For *random* cleavage with $\rho_c = 1$, the steady state is characterized by the average number $\langle N_T \rangle = J_c/\omega_c \approx (\kappa_{on} C_T - \omega_{off,T})/\omega_c$ for large C_T. For *vectorial* cleavage with $\rho_c = 0$, the number $\langle N_T \rangle$ increases monotonically with C_T and diverges at the threshold $C_{T,c}$; see Fig. 4(a).

Furthermore, as shown in [22], *strongly cooperative* cleavage leads to the singular behavior

$$\langle N_T \rangle \approx \sqrt{\pi}\kappa_{on} C_T / \sqrt{2\omega_{cD}\omega_{cT}} \tag{6}$$

for small $\omega_{cT} = \rho_c \omega_c$ provided $C_T > C_{T,c}$, compare (4). The singular behavior of $\langle N_\Theta \rangle$ is described in [22].

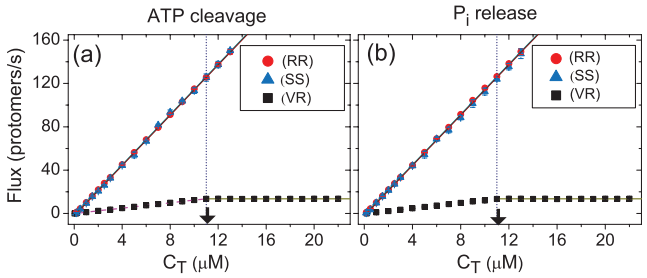

FIG. 3 (color). Total ATP cleavage flux J_c and total P_i release flux J_r in units of protomers/s versus actin concentration C_T. The full circles (red), up-triangles (blue), and full squares (black) are obtained for the three processes (RR), (VR), and (SS) as defined in Table I. The black arrow indicates the threshold concentration $C_{T,c} = 11.0\mu M$ for vectorial cleavage.

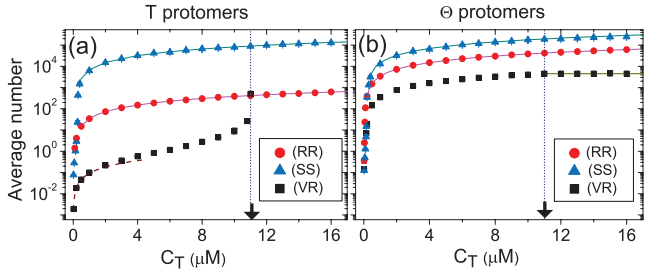

FIG. 4 (color). Average numbers $\langle N_T \rangle$ and $\langle N_\Theta \rangle$ of T and Θ protomers as a function of actin concentration C_T for the three processes (RR), (VR), and (SS); compare Table I. For process (VR) corresponding to vectorial cleavage with $\rho_c = 0$, the average number of T protomers diverges at the threshold concentration $C_{T,c} = 11.0\mu M$.

Depolymerization after dilution.—We now address the recent depolymerization after dilution experiments in [14]. In these experiments, F-actin was first grown in an ATP-actin solution with $C_T = 6\mu M$ [24] for about 1 min in the presence of filamin at the chamber walls. The filamin acts as a crosslinker that immobilizes some of the filaments at the walls. The solution was then diluted by perfusion of the chamber washing out remaining G-actin and unattached filaments. After this dilution step, which took 0.5–2 min, single filaments immobilized at the chamber walls were imaged by fluorescence microscopy, which allowed to measure their length as a function of time. For two filaments denoted by f_1 and f_2 in [14], this time evolution of the filament length was reported for 2000 s as shown in Fig. 1.

We have simulated these processes as follows. First, we grow filaments for 1 min at $C_T = 6\mu M$. We then set $C_T = 0$ and wait for a variable dilution time before we monitor the subsequent time evolution of the filament length. Using the process (SS) with dilution times of 50 and 75 s for f_1 and f_2, respectively, we obtain very good agreement with the experimental data of [14]; see Fig. 1. We also performed the same type of simulations for the processes (RR) and (VR). The resulting depolymerization curves are also included in Fig. 1 and are completely different from the one observed experimentally. In general, we find three distinct dynamic phases of depolymerization for strongly cooperative subprocesses with $0 \leq \rho_c \lesssim 10^{-3}$ and $0 \leq \rho_r \lesssim 10^{-3}$.

Our conclusions remain unchanged if we include the slow shrinkage rate at the pointed end as well. In [14], the latter rate was estimated to be 0.11 ± 0.04 protomers/s. Thus, we also performed simulations for process (SS), when all detachment rates in Table I were increased by 0.1 protomers/s, and found again rather good agreement with the data in [14].

Summary.—We introduced and studied a new theoretical model for cooperative ATP cleavage and P_i release by actin protomers. The cooperativity is described by two dimensionless parameters, ρ_c and ρ_r; see (2) and (3). Random subprocesses are obtained for $\rho_c = 1$ and/or $\rho_r = 1$, vectorial ones for $\rho_c = 0$ and/or $\rho_r = 0$. The recent experimental observations in [14] are explained by strongly cooperative ATP cleavage followed by strongly cooperative P_i release; see Fig. 1. To determine the dependence of this cooperativity on the ionic conditions, further experiments would be very valuable.

*URL: http://www.mpikg.mpg.de/th/
[1] D. Bray, *Cell Movements* (Garland Publ., New York, 2001).
[2] L. Otterbein, P. Graceffa, and R. Dominguez, Science **293**, 708 (2001).
[3] P. Graceffa and R. Dominguez, J. Biol. Chem. **278**, 34 172 (2003).
[4] M. Rould, Q. Wan, P. Joel, S. Lowey, and K. Trybus, J. Biol. Chem. **281**, 31 909 (2006).
[5] A. Orlova, A. Shvetsov, V. E. Galkin, D. S. Kudryashov, P. A. Rubenstein, E. H. Egelman, and E. Reisler, Proc. Natl. Acad. Sci. U.S.A. **101**, 17 664 (2004).
[6] E. Reisler and E. H. Egelman, J. Biol. Chem. **282**, 36 133 (2007).
[7] T. Pollard and A. Weeds, FEBS Lett. **170**, 94 (1984).
[8] D. Pantaloni, T. Hill, M.-F. Carlier, and E. Korn, Proc. Natl. Acad. Sci. U.S.A. **82**, 7207 (1985).
[9] M.-F. Carlier, D. Pantaloni, and E. Korn, J. Biol. Chem. **262**, 3052 (1987).
[10] T. Ohm and A. Wegner, Biochim. Biophys. Acta **1208**, 8 (1994).
[11] R. Melki, S. Fievez, and M.-F. Carlier, Biochemistry **35**, 12 038 (1996).
[12] L. Blanchoin and T. Pollard, Biochemistry **41**, 597 (2002).
[13] I. Fujiwara, D. Vavylonis, and T. Pollard, Proc. Natl. Acad. Sci. U.S.A. **104**, 8827 (2007).
[14] H. Y. Kueh, W. M. Brieher, and T. J. Mitchison, Proc. Natl. Acad. Sci. U.S.A. **105**, 16 531 (2008).
[15] K. C. Holmes, D. Popp, W. Gerhard, and W. Kabsch, Nature (London) **347**, 44 (1990).
[16] M. Bindschadler, E. Osborn, C. D. Jr., and J. McGrath, Biophys. J. **86**, 2720 (2004).
[17] D. Vavylonis, Q. Yang, and B. O'Shaughnessy, Proc. Natl. Acad. Sci. U.S.A. **102**, 8543 (2005).
[18] E. Stukalin and A. Kolomeisky, Biophys. J. **90**, 2673 (2006).
[19] H. Flyvbjerg, T. Holy, and S. Leibler, Phys. Rev. Lett. **73**, 2372 (1994).
[20] D. Gillespie, J. Phys. Chem. **81**, 2340 (1977).
[21] In general, the cooperative subprocesses may involve larger neighborhoods; compare [9,19], which would, however, introduce additional model parameters.
[22] See EPAPS Document No. E-PRLTAO-103-010932. For more information on EPAPS, see http://www.aip.org/pubservs/epaps.html.
[23] The two-state model studied in [19] for microtubule catastrophes also led to small parameters $\sim 10^{-5}$.
[24] H. Y. Kueh (private communication).